

## METALLICITY GRADIENTS IN X-RAY CLUSTERS OF GALAXIES

SABRINA DE GRANDI

Osservatorio Astronomico di Brera, Via Bianchi 46, I-23807 Merate (LC), Italy

AND

SILVANO MOLENDI

Istituto di Fisica Cosmica, CNR, via Bassini 15, I-20133 Milano, Italy

*Accepted for publication in ApJ*

## ABSTRACT

We present the projected metallicity profiles for a sample of 17 rich galaxy clusters observed by BeppoSAX. We find that the 8 non-cooling flow clusters have flat metallicity profiles. On the contrary, a strong enhancement in the abundance is found in the central regions of the cooling flow clusters. All the non-cooling flow clusters present evidence of recent merger activity suggesting that the merger events redistributes efficiently the metal content of the intracluster medium. For the cooling flow clusters with better statistics and available optical data (A85, A496, A2029 and Perseus) we have tested whether the observed abundance excess is due to metals ejected from the galaxies located in the cluster core. We find that at a resolution  $\gtrsim 100$  kpc the observed projected abundance excess profiles are consistent with originating from a deprojected metal excess distribution tracing the optical light distribution. In the one case (i.e. Perseus) with higher resolution ( $\sim 50$  kpc), we find that the observed metal abundance excess distribution is broader than the predicted one. Such a difference can be reconciled if we assume that the metals have drifted away from their parent ejecting galaxies by a few tens of kpc, or, alternatively, if we assume that the cluster light profile has become significantly more centrally peaked because of the formation process of the central dominant cluster galaxy since the last major merger occurred.

*Subject headings:* X-rays: galaxies: abundance — intergalactic medium — Galaxies: clusters: general — cooling flows.

## 1. INTRODUCTION

The X-ray spectra of clusters of galaxies is rich in emission lines due to K and L-shell transitions from highly ionized heavy elements, the most prominent is generated by iron at about 6.9 keV. From the measure of the equivalent width of the lines it is possible to derive the abundance of the emitting elements in the gas. For rich clusters between redshift 0.3 and the present day the observed abundance of iron is about 1/3 the solar value (e.g., Mushotzky & Loewenstein 1997, Fukazawa et al. 1998, Allen & Fabian 1998 (AF98)), suggesting that a significant fraction of the intracluster medium (ICM) has been processed into stars already at intermediate redshift.

Arnaud et al. (1992) showed that the iron mass in the ICM is highly correlated with the optical light from ellipticals and lenticulars suggesting that early-type galaxies are the major source of the enrichment of the ICM. The metal enrichment mechanisms for the ICM remain controversial. Mushotzky et al. (1996) and Mushotzky & Loewenstein (1997) showed that the relative abundance of elements is consistent with an origin of all the metals in Type II supernovae (SN), supporting the proto-galactic winds scenario for the metal enrichment of the ICM. However, other works on ASCA data (Ishimaru & Arimoto 1997, Fukazawa et al. 1998, Finoguenov, David & Ponman 2000, Dupke & White 2000), still indicating a predominance of the Type II SNe enrichment at large radii in clusters, do not exclude that as much as 50% of the iron in clusters could come from Type Ia SNe ejecta in the inner parts of the clusters. Very recent observations with XMM EPIC (Böhringer et al. 2000;

Tamura et al. 2000) provide strong evidence in favor of a substantial contribution of SN Ia in the enrichment of the ICM.

X-ray observations show that in the central region of 70 – 90 per cent of the clusters the cooling time of the ICM is less than a Hubble time (e.g., Peres et al. 1998 (P98)) and that, under gravity and thermal pressure, the gas cools and flows inwards to maintain pressure equilibrium. This process is known as a cooling flow (see Fabian 1994 for a review). An interesting result found by AF98 shows that the metallicity depends on whether or not a cluster has a cooling flow. In particular, cooling flow clusters have metallicity  $\sim 1.8$  times higher than that of the non-cooling flow systems. AF98 suggest that this is caused by the presence of metallicity gradients in the cooling flow clusters.

Spatially resolved abundance measurements in galaxy clusters are of great importance because they can be used to measure the precise amount of metals in the ICM and to constrain the origin of metals both spatially and in terms of the contribution of different type of SNe as a function of the position in the cluster. Abundance gradients have been measured for a few clusters. Early works on individual objects include that on the Centaurus cluster (Fukazawa et al 1994), Hydra A (Ikebe et al. 1997), AWM7 (Ezawa et al. 1997), Perseus cluster (Arnaud et al. 1994, Molendi et al. 1998), and Virgo (Matsumoto et al. 1996, Guainazzi & Molendi 1999). Later works on cluster samples from ASCA data are those of White (2000) on a sample of 106 clusters, Dupke & White (2000) on 3 clusters, and Finoguenov et al. (2000) on 11 clusters.

A combination of good angular and energy resolution is required to resolve the metallicity distribution. The spectral range of ASCA reaches energies up to 10 keV, which are typical for hot clusters, but its point-spread function (PSF) has a large ( $\sim 2'$ ) half-power radius (HPR) that depends strongly upon the energy (Serlemitsos et al. 1995). A better combination of the properties required is provided by the Medium Energy Concentrator Spectrometer (MECS, Boella et al. 1997a) on board the BeppoSAX satellite (Boella et al. 1997b) working in the 1-10 keV with a PSF of  $\sim 1'$  (HPR), varying only weakly with the energy (D'Acri, De Grandi & Molendi 1998), and a spectral resolution of  $\sim 8\%$  at 6 keV.

In this paper we present spatially resolved metal abundance measurements for a sample of 17 rich and nearby ( $z \lesssim 0.1$ ) X-ray clusters observed with BeppoSAX. These are all the clusters with on-axis pointings and exposure times larger than 30 ks which were available at the BeppoSAX SDC archive at the end of August 2000. The observation log for the cluster sample is given in Table 1.

We have already published the metallicity measurements for some of these clusters (Perseus, Molendi et al. 1998; A2319, Molendi et al. 1999; A2029, Molendi & De Grandi 1999; PKS0745-191, De Grandi & Molendi 1999a; A3266, De Grandi & Molendi 1999b; A2256, Molendi, De Grandi & Fusco-Femiano 2000; A3562, Ettori et al. 2000). Here, for the first time, we explore systematically the relationship between metallicity gradients in the ICM in clusters of galaxies and the presence of a cooling flow.

Very recently, after this paper was submitted we have learned that Irwin & Bregman (2000) obtained metallicity gradients for a sample of 12 galaxy clusters observed by BeppoSAX. Their work differs from ours in three major ways: their sample is smaller than ours; they study profiles out to 9 arcmin only from the cluster core while we extend our analysis further out; and, finally, they do not investigate the difference between cooling flow and non-cooling flow clusters in such a systematic fashion as we do.

Unless otherwise stated, all uncertainties quoted in this paper are 68% confidence levels for 1 interesting parameter ( $\Delta\chi^2 = 1$ ). The abundances estimated are all relative to the cosmic values given in Anders & Grevesse (1989). Throughout this paper, we assume  $H_0 = 50 \text{ km s}^{-1} \text{ Mpc}^{-1}$ ,  $\Omega = 1$  and  $\Lambda = 0$ .

## 2. OBSERVATION AND DATA ANALYSIS

Standard reduction procedures and screening criteria have been applied using SAXDAX package under FTOOLS environment, to produce equalized and linearized MECS event files. Moreover all events occurring at times when the instantaneous pointing direction differs by more than  $10''$  from the mean pointing direction have been rejected.

Albeit small, the PSF-induced spectral distortions (D'Acri et al. 1998) have been taken into account using appropriated effective area files produced with the EFFAREA program, as described in Molendi et al. (1999). All MECS spectra have been background subtracted using spectra extracted from blank sky event files in the same region of the detector as the source. All spectral fits have been performed using XSPEC Ver. 10.00.

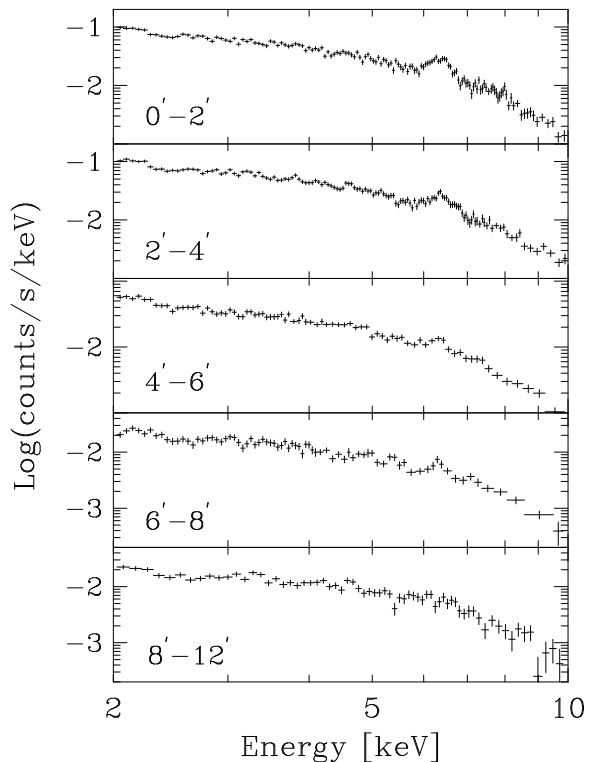


FIG. 1.— MECS spectra extracted from five concentric annular regions in the cooling flow cluster A85. Minimum and maximum bounding radii for the five regions are reported in each panel. The Fe-K $\alpha$  emission line at 6.9 keV declines rapidly with the radius.

Each cluster has been divided into concentric annuli centered on the X-ray emission peak; out to  $8'$  we accumulate spectra from 4 annular regions each  $2'$  wide, beyond this radius we accumulate spectra from annuli  $4'$  wide. For each cluster the radial profile stops at the last annulus where the intensity of the source at about 7 keV is roughly equal to that of the background. The range adopted for spectral fitting is 2-10 keV except for the  $8'$ - $12'$  annulus, where the correction for the strongback is most important. Here we restrict ourselves to the range 3.5-10 keV to avoid the low energy part of the spectrum where the correction is less reliable.

The dominant contribution to the MECS background at energies larger than  $\sim 5$  keV is from events induced by the interaction of high energy particles with the structure surrounding the instrument. Using data acquired during occultations of the satellite from the dark earth, Vecchi et al. (1999) have monitored the non X-ray background finding that variations are typically contained within  $\sim 5\%$  from the mean. In the present work, we have decided to account for these variations by excluding from our analysis spectra from the outermost regions not satisfying the conditions on the intensity of the source with respect to the background indicated in the previous paragraph. We believe that this is preferable to the alternative choice of using this data and including a systematic component to the error budget to account for possible variations in the background, the reason being that if such a component exists and is truly systematic it will show up again when we average our metallicity profiles (see Fig. 4). For the spectra which satisfy the conditions on the intensity of the source with respect to the background indicated in the previous paragraph, fluctuations of the background of up to

$\sim 5\%$  do not introduce a quantifiable increase in the error of the abundance measurement.

We have divided our clusters into a subsample of non-cooling-flow (non-CF) and cooling-flow (CF) objects on the basis of the ROSAT analysis presented in P98. For the non-CF systems we fit each spectrum with an isothermal plasma in collisional equilibrium at the redshift of the cluster (*mekal* model in XSPEC), absorbed by the nominal Galactic column density (Dickey & Lockman 1990; *wabs* model). The free parameters are the temperature ( $kT$ ) and metallicity ( $Z$ ) of the gas and the normalization.

Given the adopted spectral range (i.e.  $E > 2$  keV in all cases) the most important emission line complex we observe is the Fe  $K_\alpha$  line blend at 7 keV. This complex is the only one to clearly stand out from visual inspection of the observed spectra (see Fig. 1). The reasons for the dominance of this complex over others are several: assuming solar ratios, Fe is one of the ten most abundant elements (e.g., Anders & Grevesse 1989); the complex is well isolated from other emission features; and, finally, it is located at an energy where the MECS have a good spectral resolution and the effective areas are still relatively large. We note that although the spectral resolution of the MECS is insufficient to resolve the Fe He-like  $K_\alpha$  line at 6.7 keV from the Fe H-like  $K_\alpha$  line at 6.9 keV, it is sufficient to clearly separate the line blend from the continuum emission (see Fig. 1), and therefore derive a robust measurement of the equivalent width of the line, which, of course, is what is required to determine the Fe abundance. From the above discussion it follows that our metallicity measurements are dominated by Fe and that they cannot be used to discriminate between enrichment entirely dominated by type II Supernovae (e.g., Mushotzky et al. 1996) or enrichment from a mix of Type II and Type Ia Supernovae (e.g., Dupke & White 2000).

For the innermost region of CF clusters we have performed spectral fits with two distinct emission models: the first is the single temperature model applied to all other regions (i.e. *mekal* model); the second includes the single temperature component plus an additional component modeling the emission from the cooling flow. This second component (*mkcflow* model) accounts for a multiphase atmosphere, which cools at constant pressure from the ambient cluster temperature. All parameters of the cooling flow component, except for the normalization parameterized in terms of a mass deposition rate, are constrained: the minimum temperature is fixed at 0.1 keV, the maximum temperature and the metallicity have been set to be equal to the temperature and metallicity of the isothermal ambient (*mekal*) component. We find no evidence for a significant variation in the metallicity if the mass deposition rate is fixed to values derived from the literature either from deprojection or spectral analysis (P98, Sarazin et al. 1998, Allen 2000).

In table 2 we report the abundance measurements derived for the  $0' - 2'$  annular region in both cases. We find that no systematic trend is present when comparing the abundances measured with a single temperature model with those obtained adding a cooling flow spectral component, and, that the two metallicities are always in agreement within  $\sim 1\sigma$ .

In general the cooling radius estimated for our CF clus-

ters by P98, is contained within the first  $0'-2'$  bin. An exception is the case of the Perseus cluster with a cooling radius of  $\sim 6'$  (P98). In this specific case we have evaluated the influence of the cooling flow on the abundances measurement in the bin  $0'-2'$ ,  $2'-4'$ ,  $4'-6'$  and  $6'-8'$ , finding that the metallicities derived using a *mekal* code with or without an additional cooling flow spectral component (*mkcflow*) are again always in agreement within  $1\sigma$ .

In the following we use the abundances estimated from the single temperature model (*mekal* code) in any annular region. The metallicity measurements for the 17 clusters are reported in Table 2.

### 3. SPATIALLY RESOLVED METALLICITY MEASUREMENTS

For each cluster we compute the mean metal abundance by fitting the radial profile with a constant. The results are reported in Table 2. The mean metallicity for the whole sample of 17 clusters is  $0.29 \pm 0.01$ , in good agreement with previous works (Edge & Stewart 1991, Fukazawa et al. 1998, AF98). The mean metallicity for the CF subsample (9 clusters) is  $0.34 \pm 0.01$ , while for the non-CF subsample (8 objects) it is  $0.25 \pm 0.01$ .

Figure 2 and 3 show the radial abundance profile for the CF and non-CF clusters, respectively. The abundances are plotted against the radius in units of  $r_{180}$ , this is the radius within which the mean enclosed density equals 180 times the critical density of the universe and approximates the virial radius of the cluster in an  $\Omega = 1$  cosmology. We compute  $r_{180}$  as in Markevitch et al. (1998) which follows the prediction given by the simulations of Evrard, Metzler & Navarro (1996):  $r_{180} = 3.95 \text{ Mpc } (T_X/10 \text{ keV})^{1/2}$ . Here  $T_X$  is the mean emission-weighted temperature derived from the temperature profile up to the maximum radius available of each cluster, in units of keV. The values of  $r_{180}$  are reported in Table 2.

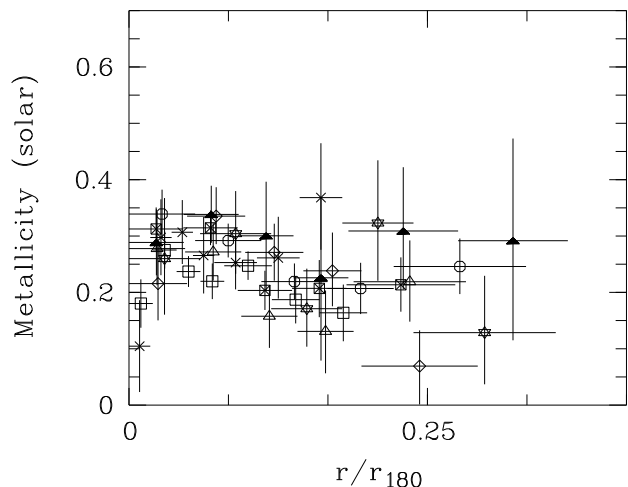


FIG. 2.— Metallicity profiles (projected) for the non-CF clusters, plotted against radii in units of  $r_{180}$ . Clusters are related to symbols as follows: A119 (lozenges), A754 (crossed squares), A2256 (circles), A2319 (filled triangles), A3266 (triangles), A3376 (stars), A3627 (crosses) and Coma (squares).

The projected abundance profiles of all the non-CF systems, plotted in Figure 2, are consistent with being constant with the radius (see Table 2). All our non-CF clusters present evidences of merger activity and/or a non-relaxed morphology in X-rays (e.g., Fabricant et al. 1993,

Mohr et al. 1995, Buote & Tsai 1996, Buote & Canizares 1996, Godlowski et al. 1998, Markevitch et al. 1998, Trevese et al. 2000, Flores et al. 2000). It seems plausible that in these clusters mergers have remixed the ICM thereby washing out any pre-existing metallicity gradient.

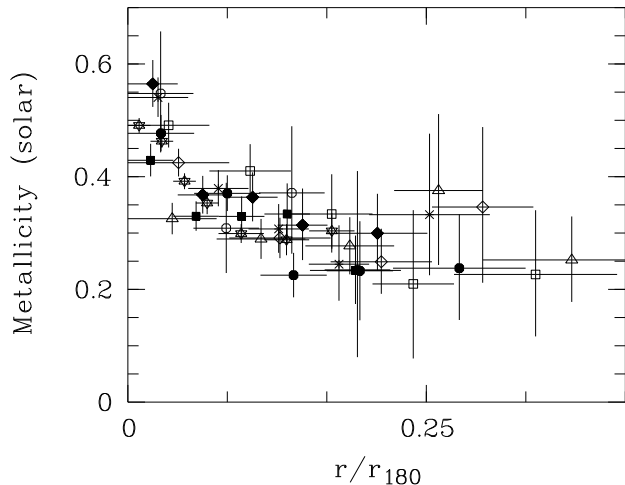


FIG. 3.— Metallicity profiles (projected) for the CF clusters, plotted against radii in units of  $r_{180}$ . Clusters are related to symbols as follows: A85 (filled circles), A496 (filled lozenges), Perseus (stars), A2029 (open squares), A2142 (open triangles), A2199 (filled squares), A3562 (open circles), 2A0335 (crosses) and PKS0745 (open lozenges).

The picture for the metallicity profiles of the CF clusters, shown in Figure 3, is completely different. A clear evidence of an abundance gradient declining with the radius is present in most of these clusters (see Table 2). Using the  $\chi^2$  statistics, a constant provides an acceptable fit only to the abundance profile for A2142 (probability of 0.78) and A3562 (probability of 0.29). A2142 is a well known cooling flow cluster with a cooling radius of about 150 kpc and a mass deposition rate  $> 300 M_{\odot} \text{ yr}^{-1}$  (P98, Allen 2000). However, several observations at optical (Oegerle, Hill & Fitchett 1995) and X-ray (Buote & Tsai 1996, Henry & Briel 1996, Markevitch et al. 2000) wavelengths indicate that this cluster is not in a dynamically relaxed state but experienced a merger event which probably failed to penetrate the core of A2142. On the other hand, for A3562 the poor statistical quality of the data is such that its abundance profile is consistent both with being constant and with having a declining profile similar to the one observed in the other CF systems.

Our individual profiles are in broad agreement with those measured by ASCA (e.g., White 2000). The most striking difference between the BeppoSAX and the ASCA results is the substantially better resolution of the former, allowing us for the first time to place tight constraints on the shape of most profiles. The most important reasons for this difference are: the better spatial resolution of the MECS and the longer exposure times of the BeppoSAX clusters (see Table 1).

#### 4. DISCUSSION

In Figure 4 we compare the mean error-weighted abundance profile for CF and non-CF clusters. The metal abundances of the CF clusters are larger than 0.4 of the solar value in the central regions and decrease rapidly to values

similar to those of the non-CF clusters at radii  $\gtrsim 0.25r_{180}$ . The profile for non-CF clusters is much flatter, a fit with a constant to all non-CF abundance measurements is statistically acceptable ( $\chi^2 = 58.8$  for 44 degrees of freedom). However, a small gradient is present in the data, indeed by performing a fit with a constant plus a linear component we find a statistically significant improvement (more than 99.5% level) according to the F-test.

The comparison of the abundance profile for CF and non-CF clusters supports the scenario where major merger events disrupt the central regions of clusters thereby remixing the gas within these regions and therefore destroying pre-existing abundance gradients. The modest gradient observed in non-CF clusters is quite likely the relic of a much stronger gradient which has not been completely wiped out by merger events.

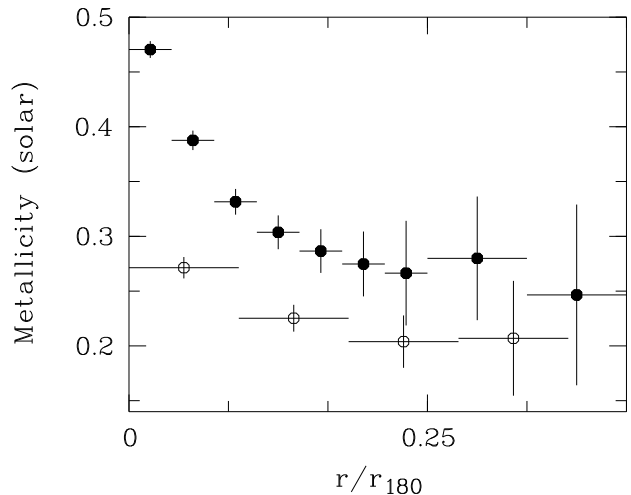


FIG. 4.— Mean metallicity profiles for the CF (filled circles) and non-CF clusters (open circles), plotted against radii in units of  $r_{180}$ .

An example of this mechanism can be found in A2256 (see Molendi et al. 2000). In this cluster a relatively recent merger event has disrupted a cooling flow that had already developed in the core of the infalling subgroups (Fabian & Daines 1991). Since the merger in A2256 is still in a relatively early stage, the remixing of the gas of the two subclusters is not complete, thereby generating an abundance gradient in the direction opposite to the merging direction.

If each merger events redistributes efficiently the metals within the ICM then the metal excess we see in the core of CF clusters should be directly related to the enrichment processes which have occurred in the cluster core since the last major merger. Thus, just as the global metallicity of clusters is an indicator of the global star formation history within the whole cluster, the abundance excess we see in the core of CF clusters is an indicator of the star formation history in the core of the cluster since the last major merger.

In the light of the above statement, we have tried to test whether the metal abundance excess we see is due to metals expelled from early type galaxies located in the core of the cluster. More specifically we have computed the metal abundance excess profile expected when the metal excess distribution traces the light distribution of early type galaxies. It can be readily shown that the projected

abundance excess  $Z_{proj}(b_{min}, b_{max})$  measured within a bin with bounding radii  $b_{min}$ ,  $b_{max}$  is related to the deprojected metal abundance excess distribution  $Z(r)$  by the following equation:

$$Z_{proj}(b_{min}, b_{max}) = \frac{\int_{b_{min}}^{b_{max}} b db \int_{b^2}^{\infty} \frac{n^2(r)Z(r)}{\sqrt{r^2 - b^2}} dr^2}{\int_{b_{min}}^{b_{max}} b db \int_{b^2}^{\infty} \frac{n^2(r)}{\sqrt{r^2 - b^2}} dr^2}. \quad (1)$$

The abundance excess is proportional to the ratio of the metal density excess, in our case iron,  $Fe(r)$ , to the gas density  $n(r)$ , i.e.  $Z(r) \propto Fe(r)/n(r)$ . If we assume that the iron excess distribution follows the distribution of light from early type galaxies,  $l(r)$ , we have  $Z(r) \propto l(r)/n(r)$ .

We have computed  $Z_{proj}$  for the 4 cooling flow objects where the metal abundance profile is best measured and optical data is available, namely: A85, A496, A2029 and Perseus (see Figure 5). X-ray and optical light density profiles  $n(r)$  and  $l(r)$  have been derived by deprojecting X-ray and optical surface brightness profiles taken from the literature. Note that we employ the total optical light profile including both the light profile of the cD and that of other early type galaxies in the core of the cluster.

All X-ray profiles are from Mohr et al. (1999), while the optical data comes from a number of works (A85: Porter et al. 1991, Slezak et al. 1998; A496: Schombert 1986, Slezak et al. 1999; A2029: Uson et al. 1991; Perseus: Schombert 1986, Brunzendorf & Meusinger 1999). Since our innermost radial bins oversample the core of the MECS PSF by a factor of 2 only, equation (1) needs to be corrected for the smoothing effects of the PSF. This is achieved by substituting the innermost integrals at the numerator and denominator with their convolutions with the MECS PSF.

In all cases the predicted abundance excess profiles show a central peak which is due to the cD galaxy. Indeed if we subtract the cD light profile from the total light profile the derived metal abundance excess profile becomes flat or even increasing with radius.

For A496 and A2029 the predicted projected metal abundance excess can be reconciled with the observed one, this is not the case for A85 and Perseus. For the latter two clusters the predicted projected metal abundance excess appears to be more centrally concentrated than the observed one. In the case of A85 the difference is not highly significant, while for Perseus the two profiles are clearly very different. We note that Perseus is the nearest cluster in our sample, if we were to move it to the redshift of the second nearest object, i.e. A496, the observed and predicted abundance excess profiles would be in broad agreement. Thus we conclude that at the resolution of a few 100 kpc the observed projected abundance excess profiles are consistent with originating from a deprojected metal excess distribution following the optical light distribution. For the one case (i.e. Perseus) where our resolution is better than 100 kpc we find that the observed abundance excess distribution is broader than the predicted one.

One possible way of reconciling the observed and predicted abundance excess profile of Perseus is to assume that metals ejected from elliptical galaxies are blown far away from them. As pointed out by Ezawa et al. (1997), the difficulty with this interpretation is that heavy ions move slowly, the typical distance covered within a Hubble time should be of the order of a few tens of kpc only. The predicted metal abundance excess profile for Perseus could

be reconciled with the observed one if the metals were to drift by about 50 kpc, this is a rather large but perhaps not impossible drift. Alternatively, if we assume that the metals have not moved far from where they have been injected in the ICM we can still explain the difference between observed and predicted profiles by noting that the optical luminosity profile we observe is the current luminosity profile, while the metal excess profile should be related to the optical luminosity profile averaged over the last few Gyrs since the cluster suffered the last major merger. Galaxies that are located at the center of clusters are thought to be formed by stripping of galaxies which fall within their gravitational attraction, therefore it is quite plausible that during such a process the light profile of a cluster has become more and more centrally concentrated. This process will inevitably lead to a current light profile which is more peaked than the light profile averaged over the time period since the last major merger and, as a consequence of this, the metal abundance excess profile predicted from the current optical light profile will be more centrally concentrated than the observed one.

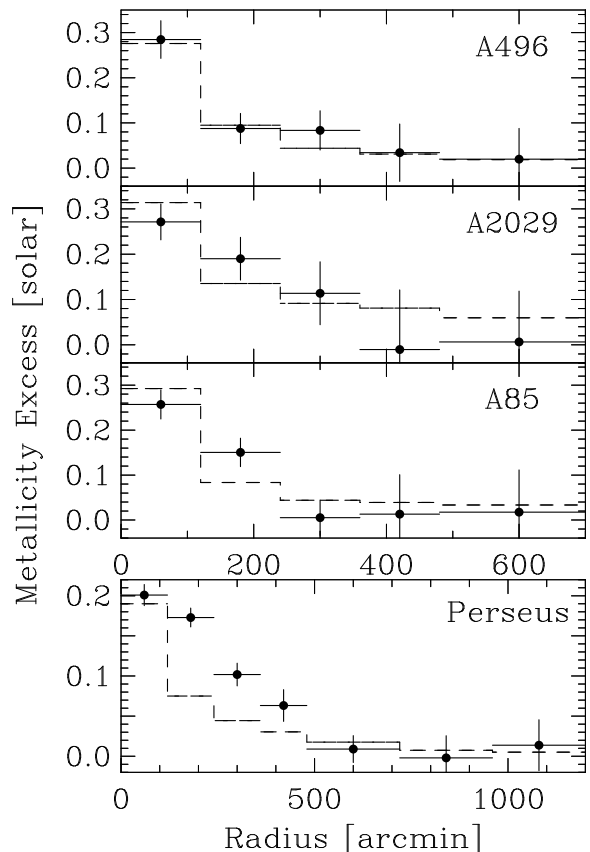


FIG. 5.— Predicted (dashed lines) versus measured (solid circles) metallicity excess profiles as a function of radius for the cooling flow clusters A496, A2029, A85 and Perseus.

We thank R. Fusco-Femiano for allowing us to use proprietary data (one observation of A754 and A119) prior to publication and the anonymous referee for his useful comments and suggestions which helped us in improving the paper. We acknowledge support from the BeppoSAX Science Data Center. Part of the software used in this work is based on the NASA/HEASARC FTOOLS and XANADU packages.

## REFERENCES

- Allen, S. W. 2000, *MNRAS*, 315, 269
- Allen, S. W., & Fabian, A., C. 1998, *MNRAS*, 297, L63 (AF98)
- Anders, E., & Grevesse, N. 1989, *Geochim. Cosmochim. Acta*, 53, 197
- Arnaud, M., Rothenflug, R., Boulade, O., Vigroux, L., Vangioni-Flam, E. 1992, *A&A*, 254, 49
- Arnaud, K. A. et al. 1994, *ApJ*, 436, L67
- Boehrer, H., Neumann, D. M., Schindler, S., Kraan-Korteweg, R. C. 1996, *ApJ*, 467, 168
- Boehrer, H., Belsole, E., Kennea, J. et al. 2000, *A&A*, in press
- Boella, G., et al. 1997a, *A&AS*, 122, 327
- Boella, G., Butler, R. C., Perola, G. C., Piro, L., Scarsi, L., & Bleeker, J. A. M. 1997b, *A&AS*, 122, 299
- Brunzendorf, J. & Meusinger, H. 1999, *A&AS*, 139, 141
- Buote, D. A. & Canizares, C. R. 1996, *ApJ*, 457, 565
- Buote, D. A. & Tsai, J. C. 1996, *ApJ*, 458, 27
- D'Acri, F., De Grandi, S., & Molendi S. 1998, *Nuclear Physics*, 69/1-3, 581 (astro-ph/9802070)
- De Grandi, S. & Molendi, S. 1999a, *A&A*, 351, L45
- De Grandi, S. & Molendi, S. 1999b, *ApJ*, 527, L25
- Dickey, J. M. & Lockman, F. J. 1990 *ARA&A*, 28, 215
- Dupke, R. A. & White R. 2000, *ApJ*, 528, 139
- Edge, A. C. & Stewart, A. C. 1991, *MNRAS*, 252, 414
- Ettori, S., Bardelli, S., De Grandi, S., Molendi, S., Zamorani, G., Zucca, E. 2000, *MNRAS*, in press
- Evrard, A. E., Metzler, C. A. & Navarro, J. F. 1996, *ApJ*, 469, 494
- Ezawa, H., Fukazawa, Y., Makishima, K., Ohashi, T., Takahara, F., Xu, H., Yamasaki, N. Y. 1997, *ApJ*, 490, L33
- Fabian, A. C. 1994, *ARA&A*, 32, 277
- Fabian, A. C. & Daines, S. J. 1991, *MNRAS*, 252P, 17
- Fabricant, D., Kurtz, M., Geller, M., Zabludoff, A., Mack, P., Wegner, G. 1993, *AJ*, 105, 788
- Finoguenov, A., David, L. P. & Ponman, T. J. 2000, *ApJ* in press (astro-ph/9908150)
- Flores, R. A., Quintana, H., Way, M. J. 2000, *ApJ*, 532, 206
- Fukazawa, Y., Ohashi, T., Fabian, A. C., Canizares, C. R., Ikebe, Y., Makishima, K., Mushotzky, R. F., Yamashita, K. 1994, *PASJ*, 46L, 55
- Fukazawa, Y., Makishima, K., Tamura, T., Ezawa, H., Xu, H., Ikebe, Y., Kikuchi, K. & Ohashi, T. 1998, *PASJ*, 50, 187
- Godlowski, W., Baier, F. W., MacGillivray, H. T. 1998, *A&A*, 339, 709
- Guainazzi, M. & Molendi, S. 1999, *A&A*, 351, L19
- Henry, J. P. & Briel, U. G. 1996, *ApJ*, 472, 137
- Ikebe, Y. et al. 1997, *ApJ*, 481, 660
- Irwin, J. A. & Bregman J. N. 2000, *ApJ*, in press (astro-ph/0009237)
- Ishimaru, Y. & Arimoto, N. 1997, *PASJ*, 49, 1
- Markevitch, M., Forman, W. R., Sarazin, C. L. & Vikhlinin, A. 1998, *ApJ*, 503, 77
- Markevitch, M., et al. 2000, astro-ph/0001269
- Matsumoto, H., Koyama, K., Awaki, H., Tomida, H., Tsuru, T., Mushotzky, R., Hatsukade, I. 1996, *PASJ*, 48, 201
- Mushotzky, R., Loewenstein, M., Arnaud, K. A., Tamura, T., Fukazawa, Y., Matsushita, K., Kikuchi, K., Hatsukade, I. 1996, *ApJ*, 466, 686
- Mushotzky, R. F. & Loewenstein, M. 1997, *ApJ*, 481, L63
- Mohr, J. J., Evrard, A. E., Fabricant, D. G., Geller, M. J. 1995, *ApJ*, 447, 8
- Mohr, J. J., Mathiesen, B. & Evrard, A. E. 1999, *ApJ*, 517, 627
- Molendi, S., Matt, G., Antonelli, L. A., Fiore, F., Fusco-Femiano, R., Kaastra, J., Maccarone, C. & Perola, C. 1998, 499, 608
- Molendi, S. & De Grandi, S. 1999, *A&A*, 351, L41
- Molendi, S., De Grandi, S., Fusco-Femiano, R., Colafrancesco, S., Fiore, F., Nesci, R. & Tamburelli, F. 1999, *ApJ*, 525, L73
- Molendi, S., De Grandi, S. & Fusco-Femiano, R. 2000, *ApJ*, 533, L43
- Oegerle, W. R., Hill, J. M., Fitchett, M. J. 1995, *AJ*, 110, 32
- Peres, C. B., Fabian, A. C., Edge, A. C., Allen, S. W., Johnstone, R. M., & White, D. A. 1998, *MNRAS*, 298, 416 (P98)
- Porter, A. C., Schneider, D. P. & Hoessel, J. G. 1991, *AJ*, 101, 1561
- Sarazin, C. L., Wise, M. W. & Markevitch, M. L. 1998, *ApJ*, 498, 606
- Serlemitsos, P. J. et al. 1995, *PASJ*, 47, 105
- Schombert, J. M. 1986, *ApJS*, 60, 603
- Slezak, E., Durret, F., Guibert, J. & Lobo, C. 1998, *A&AS*, 128, 67
- Slezak, E., Durret, F., Guibert, J. & Lobo, C. 1999, *A&AS*, 139, 559
- Tamura, T., Kaastra, J. S., Peterson, J. R. et al. 2000, *A&A*, in press
- Trevese, D., Cirimele, G., De Simone, M. 2000, *ApJ*, 530, 680
- Uson, J. M., Boughn, S. P. & Kuhn, J. R. 1991, *ApJ*, 369, 46
- Vecchi, A., Molendi, S., Guainazzi, M., Fiore, F., Parmar, A. N. 1999, *A&A*, 349, L73
- White, D. A. 2000, *MNRAS*, 312, 663
- White, D. A., Jones, C., & Forman, W. 1997, *MNRAS*, 292, 419

TABLE 1  
OBSERVATION LOG FOR THE BEPPoSAX CLUSTER SAMPLE<sup>a</sup>

Target Name	RA(2000) (degree)	DEC(2000) (degree)	Obs.Date yy-mm-dd	Obs.Code	Duration (ks)
A85	10.3750	-9.3833	1998-07-18	60632001	93
A119	14.0667	-1.2494	2000-07-05	61091002	128
A426 (Perseus)	49.9550	41.5075	1996-09-19	60009001	80
A496	68.4071	-13.2619	1998-03-05	60477001	92
A754	137.3421	-9.6878	2000-05-06	60936001	62
	137.3375	-9.6900	2000-05-17	61091001	123
A1656 (Coma)	194.8950	27.9450	1997-12-28	60126002	68
	194.8950	27.9450	1998-01-19	601260021	24
A2029	227.7313	5.7439	1998-02-04	60226001	42
A2142	239.5833	27.2333	1997-08-26	60169002	102
A2199	247.1592	39.5514	1997-04-21	60169001	101
A2256	255.9929	78.6419	1998-02-11	60465001	81
	255.9929	78.6419	1999-02-25	60126003	51
A2319	290.3025	43.9494	1997-05-16	60226002	40
A3266	67.8379	-61.4444	1998-03-24	60539002	76
A3376	90.4058	-39.9903	1999-10-17	60936002	110
A3562	203.4100	-31.6700	1999-01-31	60638001	46
A3627	243.5917	-60.8722	1997-03-01	60180001	34
2A 0335+096	54.6458	9.9650	1998-09-11	60675001	105
PKS 0745−191	116.8792	-19.2958	1998-10-23	60539001	92

<sup>a</sup>Multiple observations of the same cluster have been merged.

TABLE 2

SUMMARY OF THE BEPPoSAX MECS METALLICITY RADIAL PROFILES,  $r_{180}$  AND MEAN METALLICITY BEST-FIT RESULTS.

Name	Z(0'-2') (solar)	Z(2'-4') (solar)	Z(4'-6') (solar)	Z(6'-8') (solar)	Z(8'-12') (solar)	Z(12'-16') (solar)	Z(16'-20') (solar)	$r_{180}$ (Mpc)	$\langle Z \rangle$ (solar)	$\chi^2/\text{dof}$
CF										
A85 <sup>a</sup>	0.48±0.03 (0.49±0.04)	0.37±0.03	0.23±0.04	0.23±0.09	0.24 <sup>+0.08</sup> <sub>-0.07</sub>	—	—	3.22	0.36±0.02	28.4/4
A426 (Perseus)	0.49±0.01 (0.48±0.01)	0.46±0.01	0.39±0.01	0.35±0.02	0.30±0.02	0.29±0.03	0.30±0.03	3.19	0.41±0.01	141.1/6
A496	0.56±0.04 (0.53±0.04)	0.37±0.03	0.36±0.04	0.31±0.06	0.30±0.07	—	—	2.59	0.40±0.02	20.4/4
A2029	0.49±0.04 (0.50±0.04)	0.41±0.05	0.33±0.07	0.21±0.13	0.23±0.11	—	—	3.44	0.42±0.03	10.2/4
A2142 <sup>b</sup>	0.33±0.03 (0.33±0.03)	0.29±0.04	0.28±0.05	0.38 <sup>+0.14</sup> <sub>-0.13</sub>	0.25 <sup>+0.08</sup> <sub>-0.07</sub>	—	—	3.63	0.30±0.02	1.8/4
A2199	0.43±0.03 (0.42±0.03)	0.33±0.03	0.33 <sup>+0.04</sup> <sub>-0.03</sub>	0.33±0.05	0.23±0.06	—	—	2.65	0.35±0.02	11.8/4
A3562 <sup>c</sup>	0.55 <sup>+0.11</sup> <sub>-0.10</sub> (0.55 <sup>+0.15</sup> <sub>-0.11</sub> )	0.31±0.08	0.37 <sup>+0.12</sup> <sub>-0.11</sub>	0.23 <sup>+0.18</sup> <sub>-0.15</sub>	—	—	—	2.82	0.37±0.05	3.8/3
2A 0335+096	0.54 <sup>+0.04</sup> <sub>-0.03</sub> (0.47±0.04)	0.38±0.03	0.31±0.04	0.24 <sup>+0.06</sup> <sub>-0.07</sub>	0.33 <sup>+0.14</sup> <sub>-0.11</sub>	—	—	2.27	0.40±0.02	25.6/4
PKS 0745-191	0.42±0.02 (0.44±0.03)	0.29±0.04	0.25±0.06	0.35 <sup>+0.14</sup> <sub>-0.13</sub>	—	—	—	3.56	0.37±0.02	13.9/3
NON-CF										
A119	0.22±0.07	0.34±0.05	0.27±0.05	0.24 <sup>+0.07</sup> <sub>-0.06</sub>	0.07 <sup>+0.06</sup> <sub>-0.07</sub>	—	—	2.94	0.24±0.03	11.2/4
A754	0.31±0.04	0.31±0.03	0.20±0.03	0.21±0.05	0.21±0.05	—	—	3.78	0.26±0.02	9.6/4
A1656 (Coma)	0.18±0.04	0.28±0.03	0.24±0.03	0.22±0.03	0.25±0.03	0.19±0.04	0.16±0.05	3.74	0.23±0.01	6.7/6
A2256	0.34±0.04	0.29±0.03	0.22±0.03	0.21±0.05	0.25±0.05	—	—	3.26	0.26±0.02	7.5/4
A2319	0.29±0.06	0.34±0.05	0.30±0.10	0.23 <sup>+0.14</sup> <sub>-0.15</sub>	0.31 <sup>+0.11</sup> <sub>-0.10</sub>	0.29±0.18	—	3.86	0.31±0.03	0.8/5
A3266	0.28±0.06	0.27±0.05	0.16±0.06	0.13±0.07	0.22±0.07	—	—	3.71	0.22±0.03	4.6/4
A3376	0.26 <sup>+0.11</sup> <sub>-0.10</sub>	0.30 <sup>+0.08</sup> <sub>-0.07</sub>	0.17±0.07	0.32 <sup>+0.11</sup> <sub>-0.10</sub>	0.13 <sup>+0.10</sup> <sub>-0.09</sub>	—	—	2.46	0.23±0.04	3.4/4
A3627	0.10±0.08	0.30±0.07	0.31±0.06	0.27±0.07	0.25±0.05	0.26±0.07	0.37±0.09	3.09	0.27±0.02	5.8/6

<sup>a</sup>Southern subcluster is excluded from the spectral analysis.<sup>b</sup>AGN at  $\sim 4'$  from the cluster center is excluded from the analysis.<sup>c</sup>A3562 hosts a modest cooling flow with a very small mass deposition rate of  $37^{+26}_{-27} \text{ M}_{\odot} \text{ yr}^{-1}$  (Peres et al. 1998).